# Mechanism of Perchlorate Formation on Boron-Doped Diamond Film Anodes

**ARTICLE** *in* ENVIRONMENTAL SCIENCE & TECHNOLOGY · DECEMBER 2011

Impact Factor: 5.33 · DOI: 10.1021/es202534w · Source: PubMed



**5 AUTHORS**, INCLUDING:

Glenn Schrader
The University of Arizona
**3** PUBLICATIONS **74** CITATIONS



James Farrell
The University of Arizona
**67** PUBLICATIONS **2,390** CITATIONS



Brian P Chaplin
University of Illinois at Chicago
**28** PUBLICATIONS **431** CITATIONS

Environmental Science & Technology

ARTICLE

pubs.acs.org/est

# Mechanism of Perchlorate Formation on Boron-Doped Diamond Film Anodes

Orchideh Azizi,[†] David Hubler,[‡] Glenn Schrader,[‡] James Farrell,[‡] and Brian P. Chaplin[*,†]

[†]Department of Civil and Environmental Engineering and Villanova Center for the Advancement of Sustainable Engineering, Villanova University, Villanova, Pennsylvania 19085, United States

[‡]Department of Chemical and Environmental Engineering, University of Arizona, Tucson, Arizona 85721, United States

S Supporting Information

**ABSTRACT:** This research investigated the mechanism of perchlorate ($ClO_4^-$) formation from chlorate ($ClO_3^-$) on boron-doped diamond (BDD) film anodes by use of a rotating disk electrode reactor. Rates of $ClO_4^-$ formation were determined as functions of the electrode potential (2.29—2.70 V/standard hydrogen electrode, SHE) and temperature (10—40 °C). At all applied potentials and a $ClO_3^-$ concentration of 1 mM, $ClO_4^-$ production rates were zeroth-order with respect to $ClO_4^-$ concentration. Experimental and density functional theory (DFT) results indicate that $ClO_3^-$ oxidation proceeds via a combination of direct electron transfer and hydroxyl radical oxidation with a measured apparent activation energy of 6.9 ± 1.8 kJ·mol$^{-1}$ at a potential of 2.60 V/SHE. DFT simulations indicate that the $ClO_4^-$ formation mechanism involves direct oxidation of $ClO_3^-$ at the BDD surface to form $ClO_3^\bullet$, which becomes activationless at potentials > 0.76 V/SHE. Perchloric acid is then formed via the activationless homogeneous reaction between $ClO_3^\bullet$ and $OH^\bullet$ in the diffuse layer next to the BDD surface. DFT simulations also indicate that the reduction of $ClO_3^\bullet$ can occur at radical sites on the BDD surface to form $ClO_3^-$ and $ClO_2$, which limits the overall rate of $ClO_4^-$ formation.

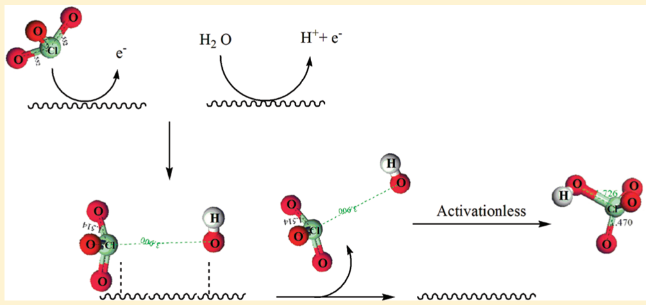


## INTRODUCTION

Boron-doped diamond (BDD) film electrodes have gained increasing interest for their ability to oxidize recalcitrant and complex aqueous waste streams.[1−5] The high oxidizing power of BDD electrodes originates from their ability to oxidize compounds by a combination of direct electron transfer reactions at the electrode surface and indirect oxidation via hydroxyl radicals ($OH^\bullet$) produced from water oxidation.[1−4,6] Various emerging water treatment applications are being developed utilizing BDD electrodes, including: treatment of landfill leachate, industrial wastewater treatment, and electrochemical disinfection of cooling tower waters, drinking water, wastewater, swimming pools, and spas.[7,8] However, the extreme promise of these electrodes for water treatment is tempered by recent studies showing the production of $ClO_4^-$ during the electrolysis of chloride-containing waters.[9−14]

The production of $ClO_4^-$ during electrolysis is problematic due to the known health risks, which include disruption of the normal function of the thyroid gland and carcinogenic potential.[15−17] These risks have prompted the U.S. Environmental Protection Agency (EPA) to issue a health advisory target of 15 parts per billion (ppb) for drinking water sources,[18] and two states, California and Massachusetts, have mandated even lower limits of 6 and 2 ppb, respectively.[15,19,20]

Recent research has shown very high concentrations of both $ClO_3^-$ and $ClO_4^-$ formed during extended electrolysis of $Cl^-$ and $ClO_x^-$ solutions by use of BDD and Pt anodes.[8−14,21] These previous studies have focused primarily on the relationship between operating conditions (e.g., temperature, flow rate, current density, and $Cl^-$ concentration) and $ClO_4^-$ formation.[9,10] It has been found that the most important parameters affecting $ClO_4^-$ formation are the mass-transfer rate to the electrode surface[9,10] and the concentration of competitive ions.[9,10,12] Low mass-transfer rates enhance $ClO_4^-$ formation due to the multistep pathway leading to its formation from $Cl^-$ as shown:

$$Cl^- \rightarrow OCl^- \rightarrow ClO_2^- \rightarrow ClO_3^- \rightarrow ClO_4^- \qquad (1)$$

where the rate-determining step in this pathway is the oxidation of $ClO_3^-$ to $ClO_4^-$.[10,21] High concentrations of competitive ions (e.g., $Cl^-$) have been shown to inhibit $ClO_4^-$ formation, due to adsorption at the electrode surface, which blocks the oxidation of $ClO_3^-$ to $ClO_4^-$.[9] Several studies have investigated the mechanisms and kinetics of $ClO_4^-$ formation on Pt, Pt/Ti, and $PbO_2$ anodes.[21−23] However, the proposed mechanisms for the formation of $ClO_4^-$ on these electrode materials are still

**Received:** July 21, 2011
**Accepted:** October 27, 2011
**Revised:** October 14, 2011
**Published:** October 27, 2011



dx.doi.org/10.1021/es202534w | Environ. Sci. Technol. 2011, 45, 10582–10590

speculative, and mechanistic studies involving $ClO_4^-$ formation on BDD electrodes have not been conducted.

Past work has shown that the functional groups on the BDD surface have a major effect on the physical, chemical, and electronic characteristics of the BDD surface and the mechanisms of both anodic and cathodic reactions.[24−26] Freshly prepared BDD surfaces are terminated with hydrogen atoms.[25,27−33] However, anodic polarization results in oxidation of some surface hydrogen atoms and produces various oxygenated functional groups,[29−35] such as carboxyl, carbonyl, and hydroxyl groups.[25,27,30−33,36,37] Evidence suggests that these oxygenated groups mediate electron transfer at BDD electrodes[24−26] and remain on the surface even after cathodic polarization.[25,38]

The aim of this work was to develop a mechanistic understanding of $ClO_4^-$ formation on BDD electrodes. Specifically, the oxidation of $ClO_3^-$ to $ClO_4^-$ was investigated as a function of electrode potential and temperature. The mechanisms of $ClO_4^-$ formation via various pathways and BDD functional groups were investigated by density functional theory (DFT) modeling.

## ■ MATERIALS AND METHODS

**Reagents.** All chemicals were reagent-grade and were obtained from Fisher Scientific. All chemicals were used as received without additional purification. All solutions were made from Milli-Q ultrapure water (18.2 MΩ·cm at 21 °C).

**Rotating Disk Electrode Experiments.** Reaction rates for $ClO_3^-$ removal and $ClO_4^-$ formation were measured at constant potential conditions by use of a rotating disk electrode (RDE) experimental setup. Currents and electrode potentials were controlled and measured with a Gamry series 6000 potentiostat/galvanostat. Experiments were performed over a temperature range of 10—40 °C by use of a circulating water bath (Thermo Electron Corp., Neslab RTE7). Ultrananocrystalline BDD films on 1.0 $cm^2$ surface area p-silicon substrates were used as the working electrode (Advanced Diamond Technologies, Romeoville, IL). Chemical vapor deposition of the BDD films was performed with a concentration of trimethylborane of 750−12 000 ppm in flowing $CH_4$, and at a temperature between 700 and 800 °C. The BDD film thickness was approximately 2 $\mu$m with a resistivity of 0.05—0.1 Ω·cm. The electrochemical cell used for RDE experiments is shown in the Supporting Information (Figure S-1). The working electrode was mounted in a custom-made poly(ether ether ketone) (PEEK) holder attached to a Pine Research Instruments rotator assembly (model AFMSRCE) and rotated at 3000 rotations per minute (rpm) to eliminate both mass-transfer limitations on the reaction rate of $ClO_3^-$ and current gradients on the BDD surface. The electrode holder exposed a 0.35 $cm^2$ electrode surface area to the electrolyte. The calculated Reynolds number was 34 800. The counterelectrode was a 12 cm long, 0.3 mm diameter Pt wire, and the reference electrode was a single-junction $Hg/Hg_2SO_4/K_2SO_4$ (mercury sulfate electrode, MSE) (Pine Research Instruments), whose internal filling solution was changed before each experiment. Anode and cathode chambers were separated by a Nafion N115 membrane (Ion Power, Inc., New Castle, DE) in order to isolate anodic and cathodic reactions. All potentials were adjusted for uncompensated solution resistance and are reported versus the standard hydrogen electrode (SHE). Experiments were conducted in 50 mL of either 10 mM or 1 M $KH_2PO_4$ buffer, pH 4.5, as a background electrolyte. Before each experiment the BDD electrode was preconditioned in a blank electrolyte solution at a current density of 20 mA·$cm^{-2}$ for 20 min to remove adsorbed species. All experiments were conducted in duplicate. Linear sweep voltammetry experiments were conducted by use of the same experimental setup as described above, except the electrode was stationary. The potential was swept from the open circuit potential to 2.74 V/SHE at a scan rate of 2 mV·$s^{-1}$, in 1.0 M $KH_2PO_4$ electrolyte, pH 4.5.

**Reaction Rate.** Two methods were used to calculate reaction rates as a function of electrode potential. In one method (current analysis), the electrode potential was stepped anodically from its open circuit potential in the blank electrolyte solution (10 mM $KH_2PO_4$, pH 4.5) to the desired potential (2.29—2.70 V), which generated a constant current for water oxidation. After 3 min, 1 mM $ClO_3^-$ was added to the electrolyte and the current increase ($\Delta i$) was recorded. The current increase was converted to a reaction rate $r$ (moles per hour) by use of Faraday's law:

$$r = \frac{\Delta i}{nF} \tag{2}$$

where $n$ is the number of electrons transferred and $F$ is the Faraday constant. Control experiments were conducted where 1 mM $ClO_4^-$ was added to the blank electrolyte in place of $ClO_3^-$. These experiments did not show a measurable current increase, indicating that the solution resistance was not significantly changed by compound addition. The choice of $ClO_4^-$ for control experiments was made because it has previously been shown to be nonreactive at BDD anodes.[39] Analytically determined reaction rates were also calculated by measuring both the disappearance of $ClO_3^-$ and formation of $ClO_4^-$ with time. Linear regression of the concentration versus time profiles was used to obtain the reaction rates. All errors reported represent 95% confidence intervals obtained by regression analysis.

**Analytical Methods.** Concentrations of $ClO_3^-$ and $ClO_4^-$ were determined by ion chromatography (Dionex ICS-3000; Dionex IonPac AS16 column; KOH eluent; 1 mL/min eluent flow rate). Free available chlorine was measured by Hach method 8021. An Accumet model 25 pH probe was used to measure the solution pH.

**Electron Transfer Coefficient.** The dimensionless electron transfer coefficient ($\alpha$) can be used to determine the rate-determining step in an electrochemical reaction mechanism. The dependence of electrochemical reaction rates on potential is described by the Butler−Volmer equation:

$$i = i_0\left[e^{\vec{\alpha}F(E - E_{eq})/RT} - e^{-\overleftarrow{\alpha}F(E - E_{eq})/RT}\right] \tag{3}$$

where $i$ is reaction current density, $i_0$ is exchange current density, $R$ is the universal gas constant, $T$ is temperature, $E$ is electrode potential, $E_{eq}$ is equilibrium potential for the redox reaction, and $\vec{\alpha}$ and $\overleftarrow{\alpha}$ are dimensionless forward (oxidation) and reverse (reduction) electron transfer coefficients, respectively. Combining eq 3 with the Nernst equation and assuming that the reverse reaction is negligible at high overpotentials[40] yields the following relationship:

$$\vec{\alpha} = \frac{-2.3RT}{F}\left(\frac{\mathrm{d}\log r}{\mathrm{d}E}\right) \tag{4}$$

where $r$ is the measured reaction rate. Plots of log $r$ versus electrode potential are used to calculate values of $\vec{\alpha}$ from the measured data.

A detailed description of how $\vec{\alpha}$ relates to a multistep electron-transfer reaction has been provided by Bockris et al.[41] The value of $\vec{\alpha}$ is a function of the number of electrons transferred before

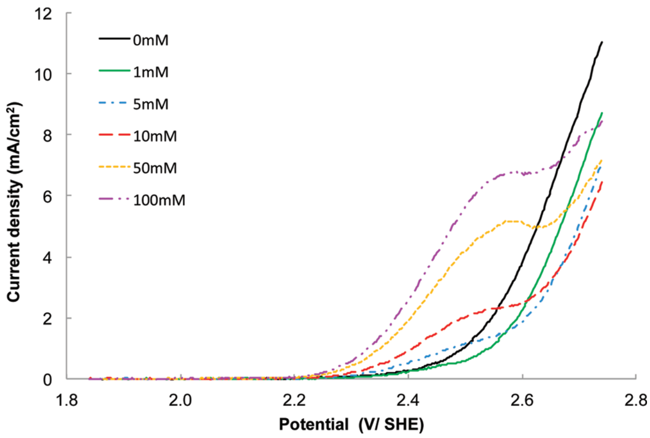


**Figure 1.** Polarization curves recorded on BDD at scan rate of 2 $mV \cdot s^{-1}$ in the absence and presence of different concentrations of $ClO_3^-$: 0, 1, 5, 10, 50, and 100 mM. Electrolyte = 1 M $KH_2PO_4$, pH 4.5.

($\vec{\gamma}$) and after ($\overleftarrow{\gamma}$) the rate-determining step, the number of times the rate-determining step occurs ($v$), and the symmetry factor ($\beta$) of the reaction.[41] Therefore, $\vec{\alpha}$ can be expressed as

$$\vec{\alpha} = \frac{\overleftarrow{\gamma}}{v} + r\beta \qquad (5)$$

where $r$ = 1 for a rate-determining step that involves direct electron transfer and $r$ = 0 for a rate-determining step that is dependent on chemical factors. The parameter $\beta$ is dependent on the symmetry of the potential energy surface between the reactant and the transition state for the rate-determining step and is close to 0.5 for a direct electron transfer reaction occurring on a metal electrode.[41]

**Quantum Mechanical Simulations.** Density functional theory (DFT) simulations were performed to investigate activation barriers for possible reactions involving $ClO_3^-$. All DFT calculations were performed with the DMol3[42,43] package in the Accelrys Materials Studio[44] modeling suite on a personal computer. All simulations used double-numeric with polarization (DNP) basis sets[45] and the gradient-corrected Becke—Lee—Yang—Parr (BLYP)[46,47] functionals for exchange and correlation. The nuclei and core electrons were described by DFT optimized semilocal pseudopotentials.[48] Implicit solvation was incorporated into all simulations by use of the COSMO-ibs model.[49] The activation energies ($E_a$) for direct electron transfer as a function of the electrode potential were calculated by the method of Anderson and Kang.[50] Reactions with the BDD electrode surface were modeled by use of a previously described 10-carbon atom cluster containing hydrogen and oxygen surface terminations.[26] Activation energies for reaction with the surface and with $OH^\bullet$ were calculated by minimizing the energy of the system for fixed distances between reacting atoms.

## RESULTS AND DISCUSSION

**Experimental Results.** Figure 1 shows linear sweep voltammetry profiles recorded on the stationary BDD electrode at a scan rate of 2 $mV \cdot s^{-1}$ in the presence of different concentrations of $ClO_3^-$ (0—100 mM) in the 1.0 M $KH_2PO_4$ supporting electrolyte. At potentials lower than those necessary for significant water oxidation, an increase in $ClO_3^-$ concentration above 5 mM leads to the appearance of an oxidation peak (~2.4—2.6 V). This peak becomes higher and shifts toward higher potentials with increasing $ClO_3^-$ concentration, providing evidence that $ClO_3^-$ reacts on the BDD surface via a direct electron-transfer reaction.[1,51] In the region of significant water oxidation (~ 2.7 V), a drop in the current is observed at all $ClO_3^-$ concentrations relative to the blank electrolyte. At a potential of 2.7 V, the current progressively decreases up to $ClO_3^-$ concentrations of 10 mM, and at $ClO_3^-$ concentrations > 10 mM the current then begins to increase. At low $ClO_3^-$ concentrations (<10 mM) the blockage of water oxidation sites by adsorbed $ClO_3^-$ (or reaction products) induces this initial current decrease. However, at higher $ClO_3^-$ concentration (>10 mM), suppression of the water oxidation reaction is compensated by increased $ClO_3^-$ oxidation, which leads to a net increase in the observed current.

Chronoamperometry experiments were performed at 21 °C to determine the rate of $ClO_4^-$ formation as a function of electrode potential. These experiments were conducted in a 10 mM $KH_2PO_4$ electrolyte, with the RDE rotated at 3000 rpm. Profiles for chronoamperometry experiments are shown in Figure S-2 in the Supporting Information. At potentials of 2.60 and 2.70 V, the injection of 1 mM $ClO_3^-$ to the electrolyte solution resulted in an increase in current compared to the blank electrolyte, providing further evidence of direct electron-transfer reactions.[1] Unlike the linear polarization experiments that showed a decrease in current in the presence of 1 mM $ClO_3^-$ relative to the blank electrolyte at these potentials, chronoamperometric experiments were conducted with a rotating electrode, which prevented mass-transfer control of $ClO_3^-$ concentrations at the BDD surface, and thus higher currents were observed. At potentials of 2.29 and 2.44 V, the total currents were similar in the presence of 1 mM $ClO_3^-$ compared to those in the blank electrolyte (Figure S-2, Supporting Information), which support the linear sweep polarization experiments shown in Figure 1.

Concentration versus electrolysis time profiles for $ClO_3^-$ removal and $ClO_4^-$ formation at potentials ranging from 2.29 to 2.70 V at a temperature of 21 °C are shown in Figure 2. Duplicate control experiments, which were conducted without an applied potential, showed that $ClO_3^-$ was removed from the anode chamber during the first 30 min of the experiment. After this time, $ClO_3^-$ concentrations were approximately constant. Analysis of the reference electrode filling solution at the completion of the experiments detected an average of 930 $\mu$M $ClO_3^-$, indicating it transferred into the reference electrode through the porous ceramic frit. The final mass balance for the control experiments was 103% with respect to the initial $ClO_3^-$ concentration. Results from the control experiments are plotted in Figure 2a, along with the $ClO_3^-$ data measured at applied potentials between 2.29 and 2.70 V. All $ClO_3^-$ data shows a similar trend for the first 30 min of reaction, due to transport into the reference electrode. Therefore, rates of $ClO_3^-$ oxidation were calculated by regressing the data at times >30 min. $ClO_3^-$ oxidation rates increased with increasing potential (0.006—1.17 $\mu mol \cdot h^{-1}$) and were not statistically different than $ClO_4^-$ formation rates (0.008—1.60 $\mu mol \cdot h^{-1}$) at the 95% confidence level (Figure 2b), indicating that $ClO_3^-$ was primarily transformed to $ClO_4^-$.

A mass balance for Cl is shown in Supporting Information for all potentials investigated (Figure S-3). The mass balance is based on summation of the measured $ClO_3^-$ and $ClO_4^-$ concentrations in each experiment and normalized to the $ClO_3^-$ concentrations measured in the control experiments. Final mass balances between 98% and 100% were found during oxidation

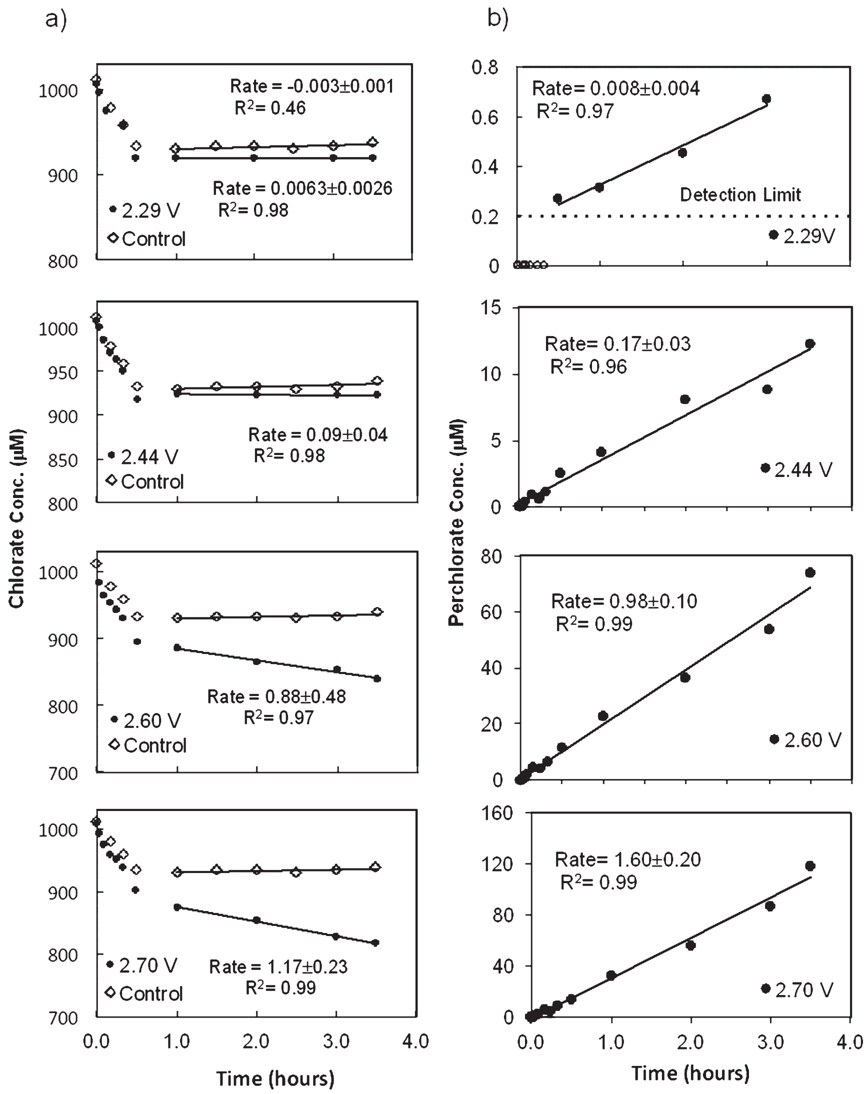


**Figure 2.** (a) $ClO_3^-$ and (b) $ClO_4^-$ concentrations as a function of time, at different anodic potentials on BDD electrode. (●) Average values of duplicate experiments; (—) linear regressions. Rate constants are presented as micromoles per hour. Experiments were conducted in 50 mL of 10 mM $KH_2PO_4$ buffer background electrolyte, pH 4.5; at 21 °C. Reported errors represent 95% confidence intervals. (◇) Control experiment conducted in the reactor without the BDD electrode. (○) $ClO_4^-$ concentrations were below the detection limit (0.2 $\mu$M) during the first 30 min of reaction at 2.29 V/SHE, and thus these data were not used in the regression.

experiments, and analysis of the liquid samples did not detect other Cl species (e.g., $Cl^-$, $Cl_2$, or $ClO_2^-$). However, the shaft of the RDE prevents a sealed reactor, and the escape of trace volatile compounds was possible under the vigorous mixing conditions employed in the experiments (3000 rpm). In previous nonelectrochemical studies, $Cl_2O_6$ (volatile species) was proposed as an intermediate in $ClO_4^-$ formation,[52] through dimerization of $ClO_3^{\bullet}$.[53] Evidence was not found to support the formation of $Cl_2O_6$, as $ClO_4^-$ formation was insensitive to the initial $ClO_3^-$ concentration (data not shown). However, its formation and subsequent volatilization from solution was possible at trace levels.

A comparison between the two methods used to calculate the reaction rates of $ClO_4^-$ formation shows that, at high oxidation potentials (2.60 and 2.70 V; Figure S-2, Supporting Information), the rates calculated by current analysis using eq 2 for a one-electron transfer reaction are 3.73 and 9.70 $\mu$mol·h$^{-1}$ at 2.60 and 2.70 V, respectively, which are approximately 4 and 6 times higher than the analytically measured $ClO_4^-$ formation rates of 0.98 and 1.60 $\mu$mol·h$^{-1}$ at these same potentials. These results indicate that additional direct electron transfer reactions involving either $ClO_3^-$ or reaction products are occurring at the BDD surface that do not directly lead to $ClO_4^-$ formation. The lack of a measurable electrode response to 1 mM $ClO_3^-$ injection at potentials of 2.29 and 2.44 V is likely due to the fact that the calculated $\Delta i$ values were 1.23 and 24.7 $\mu$A·cm$^{-2}$, respectively, which were determined by plugging the analytically measured rates into eq 2. These values are comparable to the variation in the measured currents, which were ±7 and ±20 $\mu$A·cm$^{-2}$ at 2.29 and 2.44 V, respectively. Total current efficiencies for $ClO_4^-$ formation from $ClO_3^-$ ranged from 2.2% to 4.0% for a two-electron transfer, indicating that the reaction is not highly favorable on the electrode surface compared to water or organic compound oxidation. For example, oxidation of *N*-nitrosodimethylamine at BDD electrodes achieved current efficiencies of 77—99% over a similar electrode potential range (i.e., 2.39—2.64 V) and substrate concentration (i.e., 1.35 mM).[3]

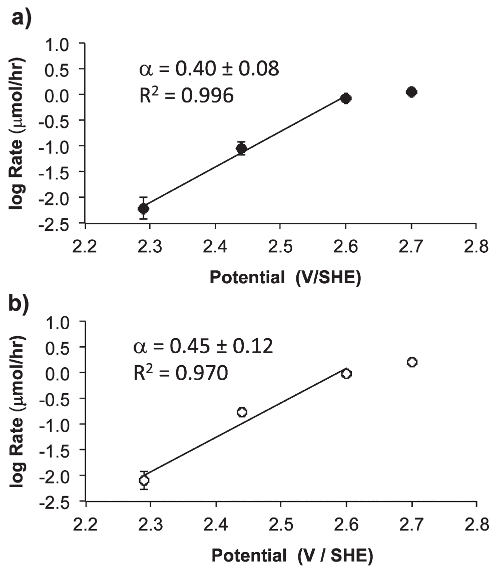


**Figure 3.** Calculation of electron-transfer coefficients by regression of (a) log rate of $ClO_3^-$ removal versus potential and (b) log rate of $ClO_4^-$ formation versus potential.

Insight into the mechanism of $ClO_4^-$ formation may be gained by examining values of $\vec{\alpha}$ obtained for $ClO_3^-$ oxidation and $ClO_4^-$ formation by use of eq 4. Values of $0.40 \pm 0.08$ and $0.45 \pm 0.12$ were obtained for $\vec{\alpha}_{ClO_3^-}$ and $\vec{\alpha}_{ClO_4^-}$, respectively (Figure 3a). The regressions shown in Figure 3 do not include the rates measured at 2.70 V, which were omitted because rates began to plateau at potentials higher than 2.60 V. This observation has been made in other studies and has been attributed to oxygen bubble formation on the electrode surface that physically blocks reaction sites[3] or to leveling off of the $OH^•$ concentration at potentials approaching 3.0 V.[54] Therefore, in order to avoid speculation on data interpretation, only potentials $\leq$ 2.60 V are considered. A value for $\vec{\alpha}_{ClO_3^-}$ = 0.40 is close to the theoretical value of $\vec{\alpha}$ = 0.5 determined by eq 5, suggesting a one-electron direct transfer reaction is the rate-determining step for $ClO_3^-$ oxidation. This finding is consistent with results from linear sweep voltammetry and chronoamperometry experiments that suggest a direct electron transfer pathway for $ClO_3^-$ oxidation (Figure 1 and Figure S-2, Supporting Information). The fact that a value of <0.5 was found for $\vec{\alpha}_{ClO_3^-}$ is likely related to an asymmetrical potential energy surface with $\beta < 0.5$. Typical values reported for $\vec{\alpha}$ for direct electron transfer reactions on BDD electrodes range from 0.3 to 0.4.[55]

The conversion of $ClO_3^-$ to $ClO_4^-$ involves an overall two-electron transfer reaction that also involves the rearrangement of chemical bonds (i.e., the addition of oxygen). The half-reaction can be written as

$$ClO_3^- + H_2O \rightarrow ClO_4^- + 2H^+ + 2e^- \tag{6}$$

A measured value of $\vec{\alpha}_{ClO_4^-} = 0.45 \pm 0.12$ was found from the rates of $ClO_4^-$ formation (Figure 3b). The similar values found for $\vec{\alpha}_{ClO_3^-}$ and $\vec{\alpha}_{ClO_4^-}$ indicate that oxidation of $ClO_3^-$ via direct electron transfer is the rate-determining step for $ClO_4^-$ formation. If transfer of the second electron was the rate-determining step, $\vec{\alpha}_{ClO_4^-}$ close to 1.5 should be observed, according to eq 5. If the overall reaction rate were limited by a chemical reaction (i.e, $r = 0$), $\vec{\alpha}_{ClO_4^-}$ close to 0 or 1.0 should be observed.

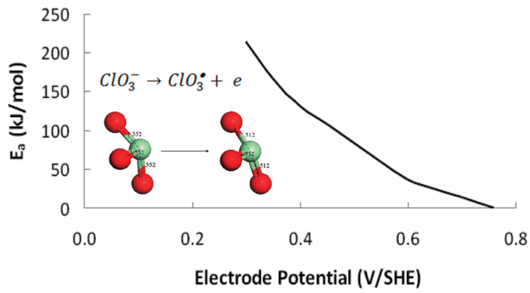


**Figure 4.** Activation barrier calculation as a function of electrode potential for direct oxidation of $ClO_3^-$. Atom key: Cl, green; O, red.

The temperature dependence of the $ClO_4^-$ formation rate was used to calculate an apparent activation energy for the oxidation of $ClO_3^-$ to $ClO_4^-$. The $ClO_4^-$ formation rate was measured at 2.60 V and temperatures from 10 to 40 °C, which yielded an apparent $E_a$ of $6.9 \pm 1.8$ kJ·mol$^{-1}$ (Figure S-4, Supporting Information). Values for $E_a$ this small are normally indicative of activationless processes,[56] such as temperature effects on the composition and thickness of the electrical double layer or the relative adsorption strengths of water and $ClO_3^-$ on the electrode surface.

**Density Functional Theory Modeling.** In order to elucidate the reaction mechanisms of $ClO_4^-$ formation, DFT simulations were used to calculate $E_a$ values for direct electron transfer from $ClO_3^-$ and for the homogeneous reaction between $OH^•$ and $ClO_3^-$. DFT results for the direct electron transfer reaction

$$ClO_3^- \rightarrow ClO_3^• + e^- \tag{7}$$

are shown in Figure 4. $E_a$ decreases as a function of the applied potential and becomes activationless at potentials > 0.76 V (Figure 4). This result is consistent with results from linear sweep voltammetry and chronoamperometry experiments and calculated values for $\vec{\alpha}$ that support a direct electron transfer pathway. DFT simulations indicate that removing an additional electron from $ClO_3^•$ did not produce a stable structure, and therefore a direct two-electron transfer reaction is not the likely pathway for $ClO_4^-$ formation. Additionally, DFT simulations indicate that the direct homogeneous reaction between $OH^•$ and $ClO_3^-$ (as shown in eq 8) did not occur, which supports experimental evidence in the literature that this reaction rate is below the quantification limit of the spin trap method (<$1 \times 10^6$ M$^{-1}$·s$^{-1}$).[57]

$$ClO_3^- + OH^• \rightarrow ClO_4^- + H^+ + e^- \tag{8}$$

Additional DFT simulations were conducted to gain information on surface complexes that may form with $ClO_3^•$. These simulations investigated the interaction of $ClO_3^•$ with different functional groups on the 10-carbon atom diamond cluster (Supporting Information, Figure S-5). X-ray photoelectron spectroscopy has identified hydrogen (≡CH), hydroxyl (≡C−OH), aldehyde (=CHO), and carbonyl (=C=O) surface terminations on BDD surfaces, where the ≡C−OH group is the most prevalent oxygenated site and has been determined to represent ~10—20% of surface groups.[30−33] Under anodic polarization, these surface functional groups may become oxidized and undergo loss of either an electron or H atom, producing surface radical sites.

DFT results indicate that $ClO_3^•$ did not chemisorb to either ≡CH or =C=O sites. The calculated $E_a$ associated with $ClO_3^•$ adsorption at a $=CHO^•$ site was 158 kJ·mol$^{-1}$. The high $E_a$

**Scheme 1. Proposed Reaction Mechanism for Formation of $ClO_4^-$ from $ClO_3^-$ on BDD Anodes**[a]

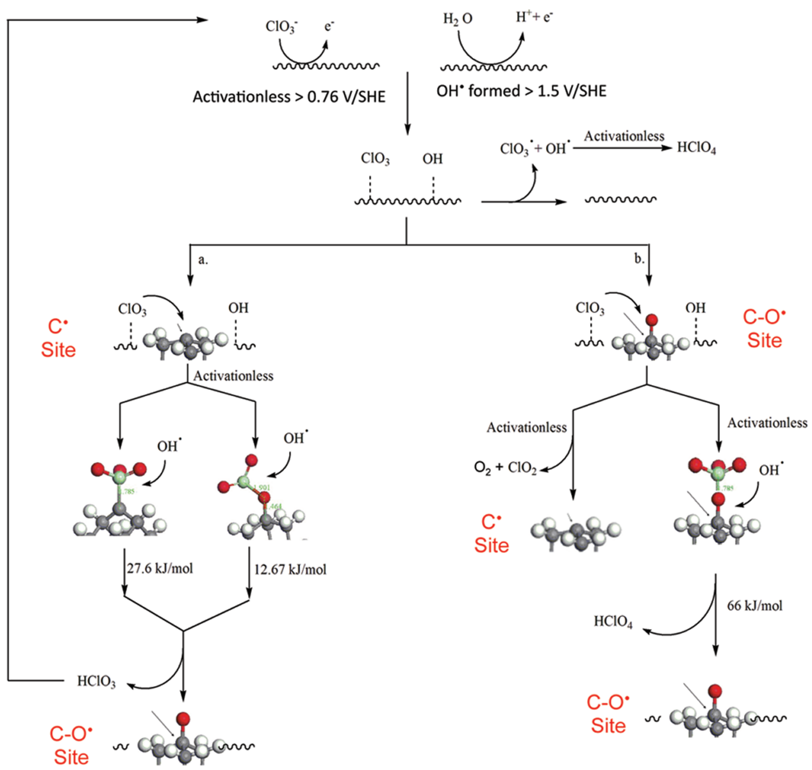


[a] Atom key: C, gray; Cl, green; H, white; and O, red. Full structure of 10-carbon diamond with different functional groups is presented in Supporting Information, Figure S-5.

indicates that it is not an important reaction site at room temperature. However, $ClO_3^•$ formed activationless chemisorbed complexes with $\equiv C^•$ and $\equiv C-O^•$ sites, indicating that at least two distinct sites on the BDD surface participate in chemisorption of $ClO_3^•$. The $\equiv C-O^•$ site may be an important site for oxygen evolution through an electrochemical desorption mechanism (eq 9). Therefore, the fact that DFT simulations indicate that $ClO_3^•$ adsorbs at this site supports the experimental results showing that low concentrations of $ClO_3^-$ (<10 mM) block water oxidation.

$$\equiv C-O^• + OH^• \rightarrow \equiv C^• + H^+ + O_2 + e^- \quad (9)$$

Other DFT simulations indicate that $ClO_3^•$ chemisorbs to the $\equiv C^•$ site by both its oxygen atom ($H_{15}C_{10}-O-ClO_2$) and by its chlorine atom ($H_{15}C_{10}-ClO_3$), as shown in Figures S-6 and S-7 in Supporting Information, respectively. Adsorption via both Cl and O atoms at the $\equiv C^•$ site is activationless, with overall reaction energies of $-32$ and $-279$ $kJ \cdot mol^{-1}$, respectively. DFT simulations involving $OH^•$ attack on chemically adsorbed $ClO_3^•$ with either bonding configuration yields $HClO_3$ as a product, which is released into solution while the oxygen remains on the BDD surface, forming a $\equiv C-O$ site, as shown in eqs 10 and 11:

$$\equiv C-OClO_2 + OH^• \rightarrow \equiv C-O + HClO_3 \quad (10)$$

$$\equiv C-ClO_3 + OH^• \rightarrow \equiv C-O + HClO_3 \quad (11)$$

The reactants and products of the reaction between physisorbed $OH^•$ and chemisorbed $ClO_3^•$ by its Cl atom at the $\equiv C-O$ site are shown in the Supporting Information (Figure S-8). The overall reaction energy for $OH^•$ attack of $ClO_3^•$ bonding via its Cl atom was $-560$ $kJ \cdot mol^{-1}$ with an $E_a$ of 27.6 $kJ \cdot mol^{-1}$, and the overall reaction energy for $OH^•$ attack of $ClO_3^•$ bonding via its O atom was $-64.6$ $kJ \cdot mol^{-1}$ with an $E_a$ of 12.7 $kJ \cdot mol^{-1}$. The relatively low $E_a$ values indicate that these reactions can occur at the temperatures in our experiments. The chemically bonded $ClO_3^•$ intermediate that subsequently reacts back to $HClO_3$ explains why the measured rate of $ClO_4^-$ production was much less than the calculated rate using eq 2. These results indicate that monitoring only the faradic current and correlating it to reaction rates is problematic and should be used with extreme caution. From a practical standpoint, this pathway also may act to limit $ClO_4^-$ formation.

Two other reactions were also found to take place at the $\equiv C-O^•$ and $=CHO^•$ sites. The first reaction involves $ClO_3^•$ reacting at the BDD surface to form $ClO_2$ and $O_2$, through coordination of $ClO_3^•$ with its oxygen atom at the $\equiv C-O^•$ and $=CHO^•$ sites. For the $=CHO^•$ site, the overall reaction energy was $-79.9$ $kJ \cdot mol^{-1}$ with an $E_a$ of 56.9 $kJ \cdot mol^{-1}$. The relatively high $E_a$ indicates that it is not an important reaction in our experiments. However, for the $\equiv C-O^•$ site the reaction was activationless and may provide an additional pathway that could limit $ClO_4^-$ formation, as shown below:

$$\equiv C-O^• + ClO_3^• \rightarrow \equiv C^• + ClO_2 + O_2 \quad (12)$$

Another possible reaction involves $OH^•$ attack on $ClO_3^•$ chemisorbed to the $\equiv C-O^•$ site. This reaction produces $HClO_4$ with an overall reaction energy of $-112$ $kJ \cdot mol^{-1}$ and a calculated $E_a$ of 66.0 $kJ \cdot mol^{-1}$. The relatively high $E_a$ compared to the measured value indicates that this mechanism does not likely contribute significantly to $ClO_4^-$ formation in our experiments.

In addition to bonding to the BDD surface, $ClO_3^{\bullet}$ may also react with $OH^{\bullet}$ in the solution adjacent to the electrode surface. The existence of $OH^{\bullet}$ in the bulk solution is unlikely since its lifetime in aqueous solution is on the order of <1 $\mu$s,[58] and thus it would not diffuse out of the boundary layer in this amount of time. The energy profiles of this reaction as a function of the Cl−OH bond length, along with the reactants and products, are shown in Figure S-9 in the Supporting Information. The DFT simulations indicate that the homogeneous reaction between $ClO_3^{\bullet}$ and $OH^{\bullet}$ is activationless and leads to $HClO_4$ formation, and thus this pathway is likely the primary contributor to $ClO_4^-$ formation in our experiments:

$$ClO_3^{\bullet} + OH^{\bullet} \rightarrow HClO_4 \tag{13}$$

Speculation that eq 13 may be involved in electrochemical perchlorate formation has been previously reported.[59]

**Perchlorate Formation Mechanism and Environmental Significance.** The proposed reaction mechanism for the formation of $ClO_4^-$ from $ClO_3^-$ on BDD anodes is summarized in Scheme 1. Over the potential range investigated in this study, the experimental and DFT results indicate that formation of $ClO_4^-$ from the oxidation of $ClO_3^-$ proceeds through a two-step mechanism. The first step involves the direct transfer of one electron from $ClO_3^-$ to the BDD anode, which becomes activationless at potentials >0.76 V. Subsequent solution-phase reaction of $ClO_3^{\bullet}$ with $OH^{\bullet}$ produced from water oxidation at potentials greater than 1.5 V[54] produces $ClO_4^-$ via an activationless pathway.

Calculations estimate that 16—26% of the $ClO_3^{\bullet}$ formed via direct electron transfer goes on to produce $ClO_4^-$. $ClO_3^{\bullet}$ forms chemisorption complexes with the BDD surface at $\equiv C^{\bullet}$ sites via an activationless step and subsequently reacts with physisorbed $OH^{\bullet}$ to produce $HClO_3$ and an oxidized surface site ($\equiv$C−O) via pathways with low to moderate $E_a$ values (12.7—27.6 kJ·mol$^{-1}$) (Scheme 1a). $ClO_3^{\bullet}$ also either chemisorbs or reacts at $\equiv C{-}O^{\bullet}$ sites on the BDD surface (Scheme 1b). The reaction between $ClO_3^{\bullet}$ and $\equiv C{-}O^{\bullet}$ produces $ClO_2$ and $O_2$ via an activationless step. Subsequent reaction of chemisorbed $ClO_3$ at the $\equiv C{-}O^{\bullet}$ site with $OH^{\bullet}$ produces $HClO_4$ via a high activation barrier step (66 kJ·mol$^{-1}$) (Scheme 1b).

The mechanistic insights provided in this study help explain the 2 orders of magnitude higher $ClO_4^-$ formation rate with BDD electrodes as compared to other electrodes (i.e., Pt, $IrO_2$, $IrO_2$−$RuO_2$) (Table S-1, Supporting Information),[9] which is primarily due to the ability of the BDD electrode to produce both $ClO_3^{\bullet}$ and $OH^{\bullet}$ at high concentrations. The resulting transformation products of $ClO_3^{\bullet}$ were found to be sensitive to specific functional groups on the BDD surface, resulting in the production of $ClO_4^-$, $ClO_3^-$, or $ClO_2$. Due to the great potential of BDD electrodes to oxidize aqueous waste streams, either electrode modifications or operational strategies will be needed to limit or eliminate $ClO_4^-$ formation. For example, the preparation of BDD electrodes with a high density of $\equiv$C−O sites may lead to sufficient side reactions that would significantly limit $ClO_4^-$ formation and thus will be investigated in future work.

Results from this study indicate that extreme caution must be taken when BDD electrodes are used for the oxidation of chloride-containing waters. Perchlorate concentrations at the end of the 3.5-h oxidation experiments ranged from 0.7 to 120 $\mu$M (70—12 000 ppb) between 2.3 and 2.7 V, respectively. These values are well over the U.S. EPA's health advisory target of 15 ppb and drinking water limits set by California and Massachusetts, 6 and 2 ppb, respectively. Studies using BDD electrodes to oxidize reverse osmosis brines and landfill leachates have documented levels of $ClO_3^-$ as high as 630 and 900 mg/L, respectively.[7,60] The waters used in these studies initially contained high levels of both dissolved organic carbon (20—300 mg/L as C) and $NH_4^+$ (200—800 mg/L), which both should scavenge the $Cl_2$ produced and thus limit final $ClO_3^-$ concentrations. While $ClO_4^-$ was not measured in these studies, the observed $ClO_3^-$ concentrations were an order of magnitude higher than the initial $ClO_3^-$ concentration used in our study (83 mg/L), indicating that $ClO_4^-$ formation likely occurred. However, research is needed to investigate the mechanisms of $ClO_4^-$ formation in complex waste streams, as prior work has indicated that $ClO_3^{\bullet}$ can react with organic compounds, which could substantially lower final $ClO_4^-$ concentrations.[4]

## ■ ASSOCIATED CONTENT

**S Supporting Information.** Nine figures and one table, showing electrochemical cell setup, chronoamperometry experiments, mass balance of RDE experiments, Arrhenius plot for $ClO_4^-$ formation, molecular structures of all compounds investigated, DFT simulations of $ClO_3^-$ oxidation on BDD, and comparison of $ClO_4^-$ formation on different electrodes. This material is available free of charge via the Internet at http://pubs.acs.org.

## ■ AUTHOR INFORMATION

**Corresponding Author**

*Phone: 610-519-4967; fax: 610-519-6754; e-mail: brian.chaplin@villanova.edu.

## ■ ACKNOWLEDGMENT

Funding for this work was provided by the National Science Foundation (CBET-0931749) and Villanova University.

## ■ REFERENCES

(1) Zhi, J. F.; Wang, H. B.; Nakashima, T.; Rao, T. N.; Fujishima, A. Electrochemical incineration of organic pollutants on boron-doped diamond electrode. Evidence for direct electrochemical oxidation pathway. *J. Phys. Chem. B* **2003**, *107* (48), 13389–13395.

(2) Carter, K. E.; Farrell, J. Oxidative destruction of perfluorooctane sulfonate using boron-doped diamond film electrodes. *Environ. Sci. Technol.* **2008**, *42* (16), 6111–6115.

(3) Chaplin, B. P.; Schrader, G.; Farrell, J. Electrochemical oxidation of *N*-nitrosodimethylamine with boron-doped diamond film electrodes. *Environ. Sci. Technol.* **2009**, *43* (21), 8302–8307.

(4) Chaplin, B. P.; Schrader, G.; Farrell, J. Electrochemical destruction of *N*-nitrosodimethylamine in reverse osmosis concentrates using boron-doped diamond film electrodes. *Environ. Sci. Technol.* **2010**, *44* (11), 4264–4269.

(5) Pacheco, M. J.; Santos, V.; Ciriaco, L.; Lopes, A. Electrochemical degradation of aromatic amines on bdd electrodes. *J. Hazard. Mater.* **2011**, *186* (2−3), 1033–1041.

(6) Kapalka, A.; Foti, G.; Comninellis, C. Investigation of the anodic oxidation of acetic acid on boron-doped diamond electrodes. *J. Electrochem. Soc.* **2008**, *155* (3), E27–E32.

(7) Anglada, A.; Urtiaga, A.; Ortiz, I. Pilot scale performance of the electro-oxidation of landfill leachate at boron-doped diamond anodes. *Environ. Sci. Technol.* **2009**, *43* (6), 2035–2040.

(8) Bergmann, M. E. H., Drinking water disinfection by in-line electrolysis-product and inorganic by-product formation. In *Electrochemistry for the Environment*; Comninellis, C., Chen, G., Eds.; Springer: New York, 2009; pp 163−205.

(9) Bergmann, M. E. H.; Rollin, J.; Iourtchouk, T. The occurrence of perchlorate during drinking water electrolysis using BDD anodes. *Electrochim. Acta* **2009**, *54*, 2102–2107.

(10) Bergmann, M. E. H.; Rollin, J. Product and by-product formation in laboratory studies on disinfection electrolysis of water using boron-doped diamond anodes. *Catal. Today* **2007**, *124*, 198–203.

(11) Murata, M.; Ivandini, T. A.; Shibata, M.; Nomura, S.; Fujishima, A.; Einaga, Y. Electrochemical detection of free chlorine at highly boron-doped diamond electrodes. *J. Electroanal. Chem.* **2008**, *612* (1), 29–36.

(12) Sanchez-Carretero, A.; Saez, C.; Canizares, P.; Rodrigo, M. A. Electrochemical production of perchlorates using conductive diamond electrolyses. *Chem. Eng. J.* **2011**, *166* (2), 710–714.

(13) Polcaro, A. M.; Vacca, A.; Mascia, M.; Ferrara, F. Product and by-product formation in electrolysis of dilute chloride solutions. *J. Appl. Electrochem.* **2008**, *38*, 979–984.

(14) Bergmann, M. E. H.; Iourtchouk, T.; Schmidt, W.; Nüske, G.; Fischer, M., Perchlorate formation in electrochemical water disinfection. In *Perchlorates: Production, Uses and Health Effects*; Matthews, L. E., Ed.; Nova Science Publishers: Hauppage, NY, 2011; pp 111−141.

(15) Urbansky, E. T.; Schock, M. R. Issues in managing the risks associated with perchlorate in drinking water. *J. Environ. Manage.* **1999**, *56* (2), 79–95.

(16) Urbansky, E. Perchlorate as an environmental contaminant. *Environ. Sci. Pollut. Res.* **2002**, *9* (3), 187–192.

(17) Lang, G.; Horanyi, G. Some interesting aspects of the catalytic and electrocatalytic reduction of perchlorate ions. *J. Electroanal. Chem.* **2003**, *552*, 197–211.

(18) *Interim drinking water health advisory for perchlorate*; EPA 822-R-08-025; U.S. Environmental Protection Agency, Washington, DC, December 2008.

(19) *Perchlorate in drinking water*; R-16-04; California Department of Health Services, Sacramento, CA, 2006.

(20) *Perchlorate fact sheet for public water suppliers*; Massachusetts Department of Environmental Protection, Boston, MA, 2006.

(21) Jung, Y. J.; Baek, K. W.; Oh, B. S.; Kang, J. W. An investigation of the formation of chlorate and perchlorate during electrolysis using Pt/Ti electrodes: The effects of pH and reactive oxygen species and the results of kinetic studies. *Water Res.* **2010**, *44* (18), 5345–5355.

(22) Munichandraiah, N.; Sathyanarayana, S. Kinetics and mechanism of anodic oxidation of chlorate ion to perchlorate ion on lead dioxide electrodes. *J. Appl. Electrochem.* **1987**, *17* (1), 33–48.

(23) Janssen, L. J. J.; Vanderheyden, P. D. L. Mechanism of anodic oxidation of chlorate to perchlorate on platinum-electrode. *J. Appl. Electrochem.* **1995**, *25* (2), 126–136.

(24) Granger, M. C.; Swain, G. M. The influence of surface interactions on the reversibility of ferri/ferrocyanide at boron-doped diamond thin-film electrodes. *J. Electrochem. Soc.* **1999**, *146* (12), 4551–4558.

(25) Girard, H.; Simon, N.; Ballutaud, D.; Herlem, M.; Etcheberry, A. Effect of anodic and cathodic treatments on the charge transfer of boron doped diamond electrodes. *Diamond Relat. Mater.* **2007**, *16* (2), 316–325.

(26) Mishra, D.; Liao, Z. H.; Farrell, J. Understanding reductive dechlorination of trichloroethene on boron-doped diamond film electrodes. *Environ. Sci. Technol.* **2008**, *42* (24), 9344–9349.

(27) Xu, J.; Granger, M. C.; Chen, Q.; Strojek, J. W.; Lister, T. E.; Swain, G. M. Boron-doped diamond thin-film electrodes. *Anal. Chem.* **1997**, *69*, 591A–597A.

(28) Holt, K. B.; Bard, A. J.; Show, Y.; Swain, G. M. Scanning electrochemical microscopy and conductive probe atomic force microscopy studies of hydrogen-terminated boron-doped diamond electrodes with different doping levels. *J. Phys. Chem. B* **2004**, *108* (39), 15117–15127.

(29) Martin, H.; Argoitia, A.; Landau, U.; Anderson, A. B.; Angus, J. C. Hydrogen and oxygen evolution on boron-doped diamond electrodes. *J. Electrochem. Soc.* **1996**, *143* (6), L133–L-136.

(30) Goeting, C. H.; Marken, F.; Gutierrez-Sosa, A.; Compton, R. G.; Foord, J. S. Electrochemically induced surface modifications of boron-doped diamond electrodes: An X-ray photoelectron spectroscopy study. *Diamond Relat. Mater.* **2000**, *9* (3−6), 390–396.

(31) Simon, N.; Girard, H.; Ballutaud, D.; Ghodbane, S.; Deneuville, A.; Herlem, M.; Etcheberry, A. Effect of H and O termination on the charge transfer of moderately boron doped diamond electrodes. *Diamond Relat. Mater.* **2005**, *14* (3−7), 1179–1182.

(32) Wang, M.; Simon, N.; Decorse-Pascanut, C.; Bouttemy, M.; Etcheberry, A.; Li, M. S.; Boukherroub, R.; Szunerits, S. Comparison of the chemical composition of boron-doped diamond surfaces upon different oxidation processes. *Electrochim. Acta* **2009**, *54* (24), 5818–5824.

(33) Wang, M.; Simon, N.; Charrier, G.; Bouttemy, M.; Etcheberry, A.; Li, M. S.; Boukherroub, R.; Szunerits, S. Distinction between surface hydroxyl and ether groups on boron-doped diamond electrodes using a chemical approach. *Electrochem. Commun.* **2010**, *12* (3), 351–354.

(34) Duo, I.; Fujishima, A.; Comninellis, C. H. Electron transfer kinetics on composite diamond ($sp^3$)-graphite ($sp^2$) electrodes. *Electrochem. Commun.* **2003**, *5* (8), 695–700.

(35) Santana, M. H. P.; De Faria, L. A.; Boodts, J. F. C. Electrochemical characterisation and oxygen evolution at a heavily boron doped diamond electrode. *Electrochim. Acta* **2005**, *50* (10), 2017–2027.

(36) Martin, H. B.; Argoitia, A.; Angus, J. C.; Landau, U. Voltammetry studies of single-crystal and polycrystalline diamond electrodes. *J. Electrochem. Soc.* **1999**, *146* (8), 2959–2964.

(37) Latto, M. N.; Riley, D. J.; May, P. W. Impedance studies of boron-doped CVD diamond electrodes. *Diamond Relat. Mater.* **2000**, *9* (3−6), 1181–1183.

(38) Notsu, H.; Yagi, I.; Tatsuma, T.; Tryk, D. A.; Fujishima, A. Introduction of oxygen-containing functional groups onto diamond electrode surfaces by oxygen plasma and anodic polarization. *Electrochem. Solid State* **1999**, *2* (10), 522–524.

(39) Iniesta, J.; Michaud, P. A.; Panizza, M.; Cerisola, G.; Aldaz, A.; Comninellis, C. Electrochemical oxidation of phenol at boron-doped diamond film electrode. *Electrochim. Acta* **2001**, *46*, 3573–3578.

(40) Bard, A. J.; Faulkner, L. R., *Electrochemical Methods: Fundamentals and Applications*; John Wiley and Sons: New York , 1980; p 718.

(41) Bockris, J. O. M.; Reddy, A. K.; Gambra-Aldeco, M. *Modern Electrochemistry*, 2nd ed.; Plenum Press: New York, 2000; Vol. 2A.

(42) Delley, B. An all-electron numerical-method for solving the local density functional for polyatomic-molecules. *J. Chem. Phys.* **1990**, *92*, 508–517.

(43) Delley, B. From molecules to solids with the DMOL3 approach. *J. Chem. Phys.* **2000**, *113*, 7756–7764.

(44) Materials Studio, v.4.2; Accelrys Corporation, San Diego, CA, 2007.

(45) Delley, B. Fast calculation of electrostatics in crystals and large molecules. *J. Phys. Chem.* **1996**, *100*, 6107–6110.

(46) Becke, A. Density-functional exchange-energy approximation with correct asymptotic-behavior. *Phys. Rev. A* **1988**, *38* (6), 3098–3100.

(47) Lee, C.; Yang, W.; Parr, R. Development of the Colle-Salvetti correlation-energy formula into a functional of the electron-density. *Phys. Rev. B* **1988**, *37* (2), 785–789.

(48) Delley, B. Hardness conserving semilocal pseudopotentials. *Phys. Rev. B* **2002**, *66* (15), No. 155125.

(49) Delley, B. The conductor-like screening model for polymers and surfaces. *Mol. Simul.* **2006**, *32*, 117–123.

(50) Anderson, A. B.; Kang, D. B. Quantum chemical approach to redox reactions including potential dependence: Application to a model for hydrogen evolution from diamond. *J. Phys. Chem. A* **1998**, *102* (29), 5993–5996.

(51) Wang, J. *Analytical Electrochemistry*, 3rd ed.; John Wiley and Sons, Inc.: Hoboken, NJ, 2006; p 250.

(52) Rao, B.; Anderson, T. A.; Redder, A.; Jackson, W. A. Perchlorate formation by ozone oxidation of aqueous chlorine/oxy-chlorine species: Role of $Cl_xO_y$ radicals. *Environ. Sci. Technol.* **2010**, *44* (8), 2961–2967.

(53) Zuo, Z. H.; Katsumura, Y.; Ueda, K.; Ishigure, K. Laser photolysis study on reactions of sulfate radical and nitrate radical with

chlorate ion in aqueous solutions - formation and reduction potential of $ClO_3^{\bullet}$ radical. *J. Chem. Soc., Faraday Trans.* **1997**, *93* (4), 533–536.

(54) Farrell, J.; Martin, F. J.; Martin, H. B.; O'Grady, W. E.; Natishan, P. Anodically generated short-lived species on boron-doped diamond film electrodes. *J. Electrochem. Soc.* **2005**, *152* (1), E14–E17.

(55) Duo, I.; Levy-Clement, C.; Fujishima, A.; Comninellis, C. Electron transfer kinetics on boron-doped diamond part I: Influence of anodic treatment. *J. Appl. Electrochem.* **2004**, *34* (9), 935–943.

(56) Smith, J. M. *Chemical Engineering Kinetics*; McGraw-Hill: New York, 1980.

(57) Buxton, G. V.; Greenstock, C. L.; Helman, W. P.; Ross, A. B. Critical review of rate constants for reactions of hydrated electrons, hydrogen atoms and hydroxyl radicals in aqueous solution. *J. Phys. Chem. Ref. Data* **1988**, *17*, 513–886.

(58) George, V. Critical review of rate constants for reactions of hydrated electrons, hydrogen atoms and hydroxyl radicals ($HO^{\bullet}/^{\bullet}O^{-}$) in aqueous solution. *J. Phys. Chem. Ref. Data* **1988**, *17*, 513–886.

(59) Bergmann, M. E. H. New results of applying diamond electrodes for water hygienization. In *Yearbook of Surface Technology*; Leuze Electronic: Bad Saulgau, Germany, 2009; pp 317−329

(60) Perez, G.; Fernandez-Alba, A. R.; Urtiaga, A. M.; Ortiz, I. Electro-oxidation of reverse osmosis concentrates generated in tertiary water treatment. *Water Res.* **2010**, *44* (9), 2763–2772.